

The tidal stream generated by the globular cluster NGC 3201

Carles G. Palau,^{1*} Jordi Miralda-Escudé,^{1,2†}

¹*Institut de Ciències del Cosmos, Universitat de Barcelona (UB-IEEC), Martí i Franquès 1, E-08028 Barcelona, Catalonia, Spain.*

²*Institució Catalana de Recerca i Estudis Avançats, E-08028 Barcelona, Catalonia, Spain.*

Accepted XXX. Received YYY; in original form ZZZ

ABSTRACT

We detect a tidal stream generated by the globular cluster NGC 3201 extending over ~ 140 degrees on the sky, using the *Gaia* DR2 data, with the maximum-likelihood method we presented previously to study the M68 tidal stream. Most of the detected stream is the trailing one, which stretches in the southern Galactic hemisphere and passes within a close distance of 3.2 kpc from the Sun, therefore making the stream highly favourable for discovering relatively bright member stars, while the leading arm is further from us and behind a disc foreground that is harder to separate from. The cluster has just crossed the Galactic disc and is now in the northern Galactic hemisphere, moderately obscured by dust, and the part of the trailing tail closest to the cluster is highly obscured behind the plane. We obtain a best-fitting model of the stream which is consistent with the measured proper motion, radial velocity, and distance to NGC 3201, and show it to be the same as the previously detected Gjöll stream by Ibata et al. We identify ~ 200 stars with the highest likelihood of being stream members using only their *Gaia* kinematic data. Most of these stars (170) are photometrically consistent with being members of NGC 3201 when they are compared to the cluster H-R diagram, only once a correction for dust absorption and reddening by the Galaxy is applied. The remaining stars are consistent with being random foreground objects according to simulated data sets. We list these 170 highly likely stream member stars.

Key words: globular clusters: individual: NGC 3201 - Galaxy: halo - Galaxy: kinematics and dynamics - Galaxy: structure.

1 INTRODUCTION

Stellar streams associated with globular clusters are formed when a cluster is tidally disrupted by its host galaxy. For a disc galaxy like the Milky Way, stars are stripped from the cluster especially when it approaches the centre of the Galaxy or crosses the Galactic disc. Each tidal shock populates the leading and trailing arms of the tidal stream, with escaped stars approximately following the orbit of the progenitor. This makes stellar streams useful tools to constrain the Galactic potential by fitting models of the stellar stream orbits to the observations, particularly if accurate observations of proper motions and radial velocities are available for the stream member stars. So far, many stellar streams have been discovered, (e.g. Grillmair & Carlin 2016; Malhan et al. 2018b; Shipp et al. 2018; Grillmair 2019). The publication of the *Gaia* Data Release 2 (GDR2) provides a promising

opportunity to discover new ones and to use the measured motions to study the Milky Way potential.

Several papers have developed methods to detect stellar streams in star catalogues with data on photometry, proper motions or radial velocities (e.g. Sanderson et al. 2015; Mateu et al. 2017; Malhan & Ibata 2018). In a previous paper (Palau & Miralda-Escudé 2019, hereafter PM19), we developed a new statistical method based on maximum-likelihood analysis designed to detect stellar streams associated with a known stellar system such as a globular cluster, when a small number of stream members appear superposed on a large catalogue of foreground stars. The method searches for a statistically significant overdensity of stars compared to a phase-space density model of the Milky Way. A stream model is constructed with free parameters that include the potential model of the Galaxy determining the orbits, plus the distance and velocity of the globular cluster within the constraints of the available observations. Numerical simulations of the stream are used to construct its phase-space density model. Then, the likelihood of each star in a catalogue is computed for the simulated model of the stream,

* E-mail: cgarcia@icc.ub.edu

† E-mail: miralda@icc.ub.edu

given the observed phase-space coordinates and their observational errors. The model-free parameters that maximize the likelihood function are obtained, and a statistical test for this best-fitting model is performed to infer whether the stream exists or not. If the statistical evidence for the stream existence is sufficient, we use the stream density model to select stars that are most likely to be stream members based on the kinematic evidence. Finally, our final selection is obtained by requiring the stars to be also compatible with the H-R diagram of the cluster, assuming the distance to each star to be that predicted by the stream model.

Applying this method to the globular cluster M68, we found a long tidal stream stretching over the North Galactic hemisphere, and passing about 5 kpc from the Sun. This stream was found to match the stellar stream named Fjörm, independently discovered by Ibata et al. (2019). For that study, absorption and reddening by Galactic dust was neglected when using the photometric observations to require stream members to be compatible with the H-R diagram of M68. We have further checked if other streams generated by globular clusters can be found in the GDR2 catalogue. Here, we study the case of NGC 3201, for which we also find a new stellar stream in which the effect of dust absorption and reddening is large and crucial for recognizing the stream members.

In Section 2 we describe NGC 3201 and our simulation of its tidal stream, and discuss the expected background using a simulation of the *Gaia* catalogue. In Section 3, our statistical method is applied to select the GDR2 star candidate members of the NGC 3201 tidal stream and to estimate its statistical significance, and we conclude in Section 4.

2 SIMULATIONS OF THE NGC 3201 TIDAL STREAM AND DETECTION METHOD

Our stream detection method, fully described in PM19, starts by computing an initial simulation of the tidal stream of NGC 3201 using a fiducial model for the Galactic potential and the central observed values of the velocity and distance to the globular cluster. Then, a bundle of possible stream models is computed by considering a range of parameter values for both the Galactic potential and the globular cluster kinematics, which is used to pre-select a sample of stars in GDR2 as possible candidates of the stream, greatly reducing the number of stars to be used in the final model fit of the stream. One important difference we will find in this work compared to our previous one on the globular cluster M68 in PM19 is that NGC 3201 is close to the Galactic plane, at $b = 8.64$ deg, with a high density of foreground stars and dust obscuration. We will start ignoring the presence of dust obscuration in this section (like we did in PM19 for the M68 tidal stream), but in the next section we shall include a model for obscuration and reddening, showing how it has substantial impact in our final selection of candidate members of the NGC 3201 tidal stream.

The NGC 3201 cluster is ~ 5 kpc away from the Sun, near the Galactic plane and at longitude $l = 277.23$ deg, and has an extreme radial velocity of 494 km s^{-1} , the highest of all globular clusters in the Milky Way, which indicates a retrograde orbit coming from a large apocentre. The implied long orbital period motivates searches for a tidal stream as-

sociated to this cluster, which may have formed from its outer envelope and not have been exposed to a large degree of phase mixing during its orbital history. Some evidence for this tidal stream has been pointed out in Chen & Chen (2010), who noted aligned star clumps of 2MASS sources in the cluster envelope. Kunder et al. (2014) obtained similar conclusions using stars with radial velocity from the RAVE survey, identifying unbound stars extending a few arc minutes away from the cluster. This was extended by Anguiano et al. (2016), who found tidal stream candidates out to ~ 80 deg from the cluster. Recent work using *Gaia* data has confirmed these observations, reporting an excess of RR Lyrae (Kundu et al. 2019) and a high velocity dispersion profile beyond the Jacobi radius together with aligned stellar over-densities near the cluster (Bianchini et al. 2019).

2.1 Initial stream simulation

We carry out a fiducial simulation of the formation and evolution of the tidal stream of NGC 3201, following the method that is described in detail in section 2.5 of PM19. Briefly, the method consists of integrating the orbits of test particles initially distributed in a fixed Plummer potential that models the globular cluster, which is at the same time orbiting in a fixed potential of the Milky Way. Initial conditions for the cluster orbit are taken from Harris (1996, 2010) for the heliocentric distance r_h , right ascension α , and declination δ , and radial velocity v_r , and we use the proper motion $\mu_{\alpha*} = \mu_\alpha \cos(\delta)$ and μ_δ from the *Gaia* catalogue (Gaia Collaboration et al. 2018). Central observed values and errors are listed in Table 1. Note that the heliocentric distance was obtained from modelling the H-R diagram, with an estimated error of 2.3 per cent, because the parallax error from *Gaia* is much larger.

The cluster orbit is integrated first as that of a test particle in the Milky Way potential model described in PM19. This model has fixed bulge and disc components, and an axisymmetric oblate dark halo with the parameters listed in Table 1, obtained as the best fit of the M68 tidal stream and other observational constraints in PM19. The parameters are a constant of proportionality $\rho_{0\text{dh}}$, a Galactic plane scale length $a_{1\text{dh}}$, a vertical scale height $a_{3\text{dh}}$, and inner slope α_{dh} and an outer slope β_{dh} . This profile is very close to an oblate NFW profile (which has $\beta_{\text{dh}} = 3$; Navarro et al. (1996)), with a concentration parameter $c = 10.4$, virial radius $r_{200} = 175.9$ kpc, a total mass $M_{200} = 6.37 \times 10^{11} M_\odot$, and an axis ratio $q = a_{3\text{dh}}/a_{1\text{dh}} = 0.87$. The corresponding potential flattening is $q_\phi = 0.94$ at the cluster position.

We plot the cluster orbit as a grey line in Galactocentric Cartesian coordinates in the top panels of Figure 1, on the x-y and x-z projections. The current cluster position and the Sun are marked as a red and blue dot, respectively. We highlight in red the section of the orbit from a time -60 Myr (trailing arm) to $+10$ Myr (leading arm) from the present time cluster position. The orbit in the v_x - v_y and v_x - v_z velocity space projections is shown in the bottom panels. Our computed orbital pericentre and apocentre of NGC 3201 and its vertical angular momentum component, listed in Table 1, are similar to the orbit of the tidal stream designated as Gjöll, discovered by Ibata et al. (2019), which has $r_{\text{peri}} = 7.96 \pm 0.22$ kpc, $r_{\text{apo}} = 31.9 \pm 4.4$ kpc, and $L_z = 2721 \pm 159 \text{ km s}^{-1} \text{ kpc}$. We shall show in this paper

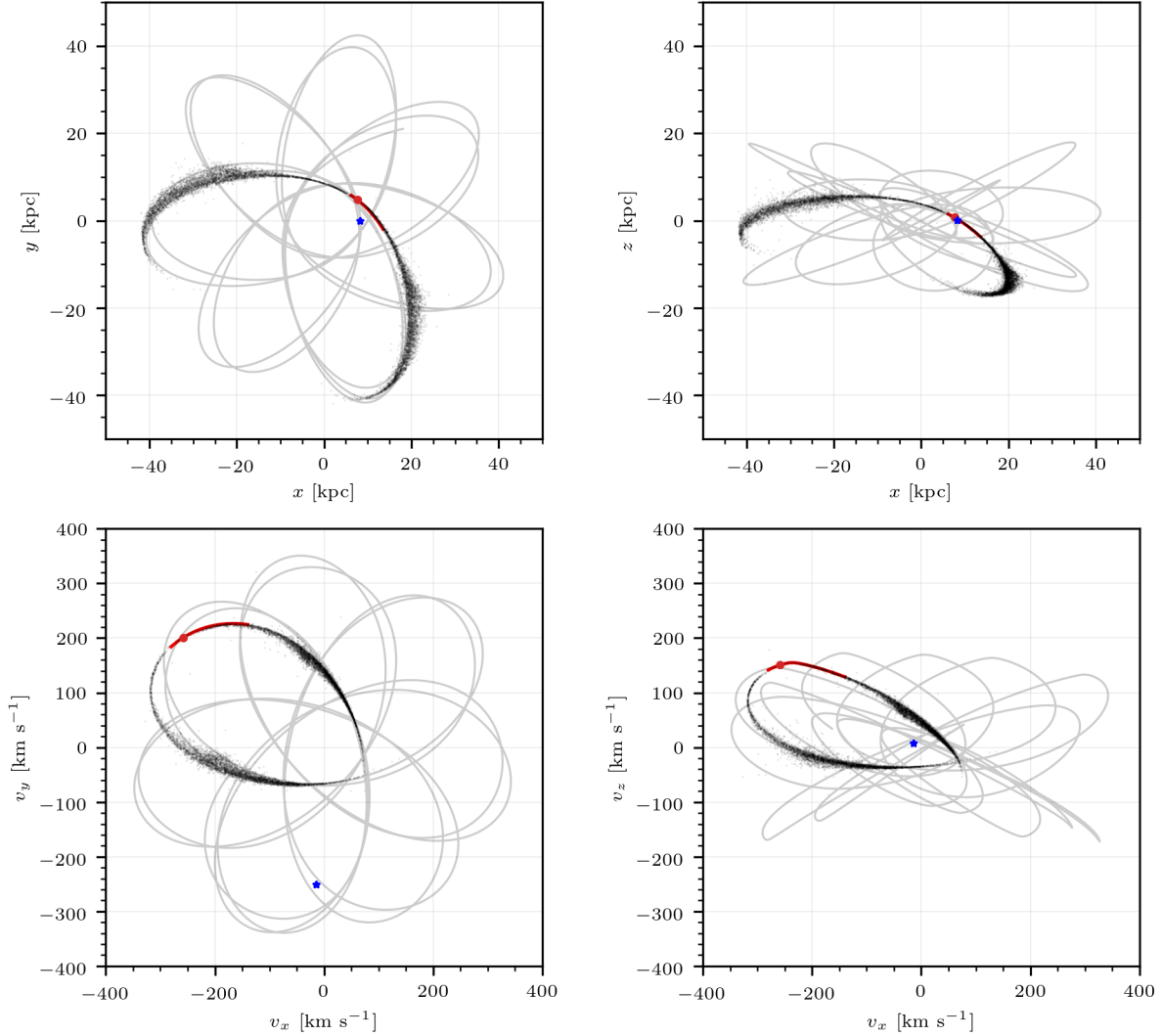


Figure 1. Computed orbit of NGC 3201 over the last 10 Gyr (grey line). The section from -60 Myr (trailing arm) to $+10$ Myr (leading arm) from the present position of the cluster (red dot) is highlighted in red. The black dots indicate the position of 10^4 tidal stream stars that have escaped the cluster potential, and the blue star is the current position of the Sun. *Top:* Projection on the Galactic disc plane (x, y) and the (x, z) plane. *Bottom:* Same projections in velocity space.

that the Gjöll tidal stream does in fact originate from the NGC 3201 globular cluster. The differences in the orbital parameters are consistent with observational and modelling uncertainties and the expected difference between the cluster orbit and the tidal stream.

We compute the orbits of 10^6 tidal stream stars as mentioned earlier and described in detail in PM19, using a fixed Plummer sphere model for the globular cluster potential with a scale parameter $a_{gc} = 4.9$ pc and a total stellar mass $M_{gc} = (6.47 \pm 0.45) \times 10^4 M_{\odot}$ from Sollima & Baumgardt (2017). In the same reference, the inferred dynamical mass for a King-Michie model is included being a factor 2 higher. An accurate estimate of the cluster mass is not relevant for our analysis since we are assuming a fixed mass throughout the evolution and the details of the phase-space distribution of the stream are not relevant to our detection method. The tidal stream orbits are started at the cluster position 10 Gyr ago, and integrated forwards in time up to the present, assuming the Plummer sphere potential follows the cluster

orbit previously computed as a test particle in the Milky Way potential, and simply adding the Plummer and Milky Way potentials. Of all the simulated stream stars that have escaped further than 0.1 deg from the cluster centre, a randomly selected subset of 10^4 of them are shown in Figure 1 as small black dots (we do not plot all of them only to better visualize their distribution). As seen in these plots, the cluster is on a relatively low inclination orbit and has recently crossed the Galactic disc moving upwards. The tidal shock it experienced may be the explanation for the overdensities observed in the cluster neighbourhood. The part of the tidal stream closest to us is the trailing arm, at ~ 4 kpc from us and 1 to 2 kpc below the disc. The large population of stars at the ends of the tidal stream is due to our initial conditions, which do not have any radial cut-off in the initial distribution of stars in the Plummer sphere, so many stars escape during the first orbits. In reality, the existence of any initial overdensities from the time the globular cluster started tidally interacting with the Milky Way depends

Table 1. Mass, core radius, present position, radial velocity, and proper motion of the NGC 3201 globular cluster. Dark halo mass density profile parameters used for tidal stream simulation, and computed cluster orbit properties.

Properties NGC 3201			Ref.
M_{gc}	(M_{\odot})	$(6.47 \pm 0.45) \times 10^4$	[1]
a_{gc}	(pc)	4.9	[1]
r_h	(kpc)	4.9 ± 0.11	[2]
δ	(deg)	-46.4125	[3]
α	(deg)	154.3987	[3]
v_r	(km s $^{-1}$)	494 ± 0.2	[2]
μ_{δ}	(mas yr $^{-1}$)	-1.9895 ± 0.002	[3]
μ_{α}	(mas yr $^{-1}$)	12.0883 ± 0.0031	[3]
Dark halo properties			
$\rho_{0\text{dh}}$	(M_{\odot} kpc $^{-3}$)	7.27×10^6	[4]
$a_{1\text{dh}}$	(kpc)	18.59	[4]
$a_{3\text{dh}}$	(kpc)	16.17	[4]
α_{dh}	-	1	[4]
β_{dh}	-	3.102	[4]
q	-	0.87	
q_{Φ}	-	0.94	
c_{200}	-	10.4	
r_{200}	(kpc)	175.9	
M_{200}	(M_{\odot})	6.37×10^{11}	
Orbit properties			
r_{peri}	(kpc)	7.71	
r_{apo}	(kpc)	43.25	
L_z	(km s $^{-1}$ kpc)	2765.45	

[1]: Sollima & Baumgardt (2017)

[2]: Harris (1996, 2010)

[3]: Gaia Collaboration et al. (2018)

[4]: PM19

on the history of the cluster and the Milky Way potential, which are likely to cause phase mixing and violent relaxation to a much greater extent than in our simple, fixed potential simulation.

The cluster orbit is shown in equatorial coordinates in the top panels of Figure 2, from 200 Myr in the past to 200 Myr in the future, as the dashed red line, with the red dot indicating the present position. The orbital path from 60 Myr ago to 10 Myr in the future is highlighted as the red solid line. We shall see that this is the part of the tidal stream where stars are most easily identified from proper motions in the *Gaia* catalogue. The Galactic centre is indicated by the grey cross, and dashed grey lines show the Galactic latitude lines at $b \pm 15$ deg. We also plot the cluster orbit in proper motion space in the bottom panels of Figure 2. The interval that is highlighted as the solid line lies in a region of higher proper motion than the rest of the orbit, which helps us to reduce the density of foreground stars and facilitates the identification of stream candidates.

2.2 Tests with the simulated *Gaia* catalogue

We now use the stars in our model tidal stream to simulate how they would be observed with *Gaia*. While computing proper motions and parallaxes from the kinematics of each star in the tidal stream is trivial, the observational errors

depend on the magnitude and colour of the stars, which we therefore need to simulate. We follow the same procedure as in PM19: we first obtain the H-R diagram of NGC 3201 from the *Gaia* data itself, by selecting a total of 7064 stars that are within 0.14 deg of the globular cluster centre and pass additional conditions specified in Appendix A. This H-R diagram is shown in Figure 3, where the derived absolute magnitude without dust correction, M'_G , computed assuming a distance $r_h = 4.9$ kpc, is plotted against the observed colour index $(G_{\text{BP}} - G_{\text{RP}})'$, and the primes generally indicate that magnitudes are not corrected for dust extinction. We randomly assign to each escaped star an absolute magnitude and colour from this H-R diagram, and compute an apparent magnitude using its simulated distance. Dust obscuration and reddening is not taken into account here, this will be included only in the next section when selecting stream candidates from the real data.

We then generate measurement error covariance matrices for the phase-space coordinates of the simulated stream stars using the Python toolkit PYGAIA¹, and following the same procedure as in section 3.2 of PM19. We assign these errors to each star, and also use them to alter the positions and velocities from the stream model by variations generated as Gaussian distributions following the same error covariance matrices. We plot as grey dots in the right-hand panels of Figure 2 the 8319 stars with G -band magnitude $G < 21$ that constitute our simulated catalogue of the stellar stream as seen by *Gaia*.

We next take a simulation of the entire *Gaia* catalogue, the 18th version of the Gaia Object Generator (GOG18; Luri et al. 2014). This catalogue includes ~ 1.5 billion sources with G -band magnitude $G \lesssim 20$, so a pre-selection of a greatly reduced sample of tidal stream candidates is necessary before we can computationally implement a maximum-likelihood method to fit a tidal stream to the candidates. We apply various pre-selection cuts as described in PM19 (Section 3.3): (1) $G < 21$, to reduce faint stars with large errors; (2) parallax $\pi > 1/0.3$ mas, to eliminate foreground disc stars; a third cut in PM19 that removed stars at low Galactic latitude is not applied here.

The fourth cut is the most important one, causing the greatest reduction in the number of star candidates. It is defined in Appendix C of PM19. Basically, we define a phase-space volume around the cluster orbit. By calculating the intersection of each star with this volume, we can choose stars close enough to the initial tidal stream model to be feasible stream stars in the final best-fitting model. We construct this volume by computing a bundle of orbits around the cluster orbit by variations of the current phase-space position of the cluster within observational errors, and variations of the Milky Way dark halo parameters. For the halo parameters, we randomly generate values following uniform distributions within the intervals: $\rho_{0\text{dh}} \sim (8 \pm 1) \times 10^6 M_{\odot} \text{ kpc}^{-3}$, $a_{1\text{dh}} \sim 20.2 \pm 4$ kpc, $a_{3\text{dh}} \sim 16.16 \pm 4$ kpc, and $\beta_{\text{dh}} \sim 3.1 \pm 0.2$. The selection threshold and the above distributions are defined such that the pre-selection criterion is broad enough to remove very few true stream stars. We require the pre-selected stars to be in the interval going from a time 60 Myr in the past to 10 Myr in the future (shown as

¹ <https://pypi.org/project/PyGaia/>

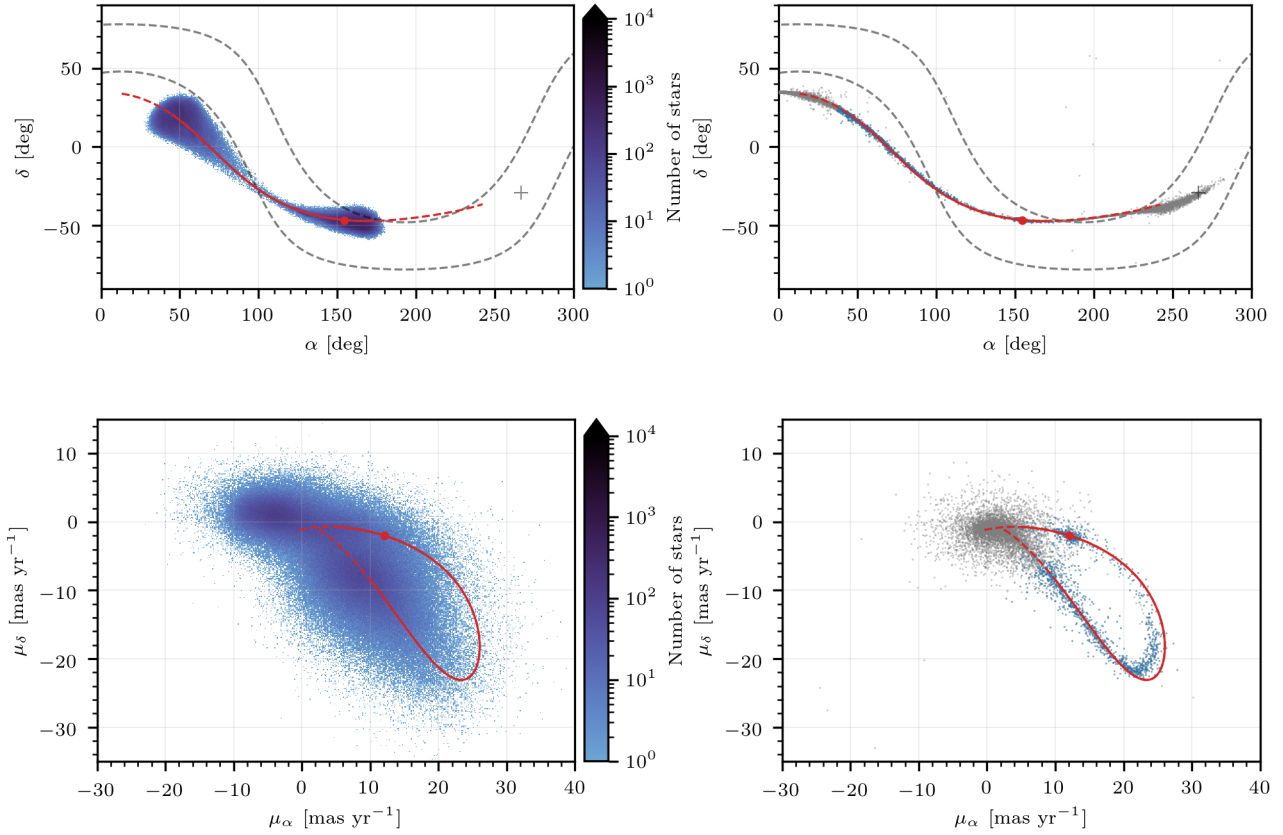


Figure 2. Computed orbit of NGC 3201, with its present position shown as the red dot, from -60 Myr to $+10$ Myr from the present (solid red line), and from -200 Myr to $+200$ Myr (dashed red line). The grey cross is the Galactic centre, and grey dashed lines mark Galactic latitude $b = \pm 15$ deg. *Left-hand panels:* Blue dots show coordinates and proper motions of stars in the GOG18 catalogue pre-selected for our search for stream candidates. *Right-hand panels:* Coordinates and proper motions of the simulated tidal stream stars are shown as blue dots if they are in our pre-selected sample, and as grey dots if they are not.

solid red line in Figures 1 and 2) because the dense stellar foreground and large distance to the stream make it difficult to find stream stars outside this interval. Finally, the fifth cut removes stars within 1.5 deg of the cluster centre, to remove stars that may still be bound to the cluster and are not part of the tidal stream.

The GOG18 pre-selected stars after these cuts (a total of 486 664, as listed in Table 2) are plotted in the left-hand panels of Figure 2 as blue dots. The right-hand panels also shows as blue dots the 1609 stars in our simulated tidal stream that pass the same pre-selection cuts. Most of the other stars in our simulated stream are eliminated because they are far from our orbital interval from -60 to 10 Myr, where detecting the candidates is more difficult. We can see how within this interval, only a few simulated stream stars have not passed these cuts (grey dots) proving that our fourth cut does not bias the selection. The density of contaminating foreground stars is minimum in the range $\alpha \in [80 - 120]$ deg, corresponding to the section of the stream closest to the Sun where the proper motion is largest. Our pre-selection volume cuts out most of the leading arm, as

well as the distant ends of the simulated stream. These cut out regions are far from the Sun, projected near the disc and with proper motions that have a high density of foreground stars. We will focus in the search for candidates in the portion of the tidal stream defined by our cuts in this paper, although other stream stars are expected to be found over the more extended, complete simulated stream in future work.

3 SELECTION AND DETECTION OF THE NGC 3201 STREAM STARS FROM GDR2

Our goal in this section is to obtain a best-fitting model of the stellar stream associated with NGC 3201 varying parameters of the Milky Way potential and the globular cluster kinematics, showing at the same time that the kinematic data of the GDR2 catalogue proves the existence of this stellar stream with a high degree of statistical confidence. A list of candidate stellar stream members that are also photometrically consistent with the NGC 3201 H-R diagram will

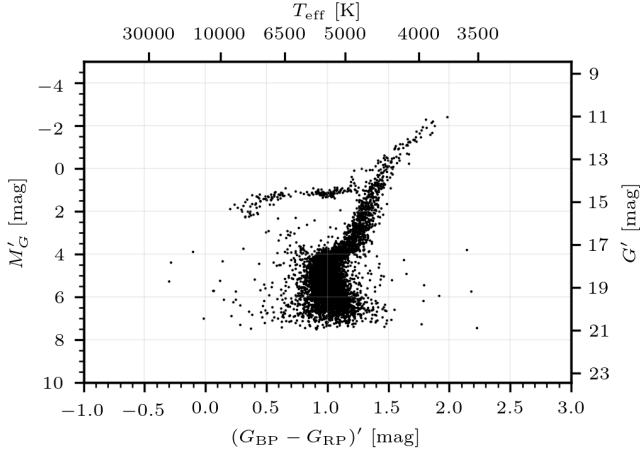


Figure 3. Absolute magnitude without dust extinction correction, M'_G versus observed $(G_{BP} - G_{RP})'$ colour index for 7064 stars within 0.14 deg of the centre of NGC 3201, selected with the conditions of the query given in Appendix A. The absolute magnitude is computed assuming a heliocentric distance $r_h = 4.9$ kpc.

be given. While each of these candidates has some probability of being a false member (a projected foreground or background star), our method relies on the statistical detection and maximizes the stream-likelihood function based on the number of candidates identified with a high membership probability.

3.1 Pre-selection of GDR2 stars

We first apply our pre-selection method to the GDR2 catalogue to reduce the number of stars used to fit the stellar stream to a computationally manageable level. This catalogue includes a total of ~ 1.7 billion sources with parallaxes, sky coordinates and proper motions, and ~ 7.2 million sources with radial velocities. The number of stars that pass each of our cuts defined in Section 2 is specified in Table 2, together with the same number for the simulated catalogue GOG18. The first two cuts (1 and 2) eliminate a small number of stars, and the main reduction is achieved in cut 4, leaving 492 983 for GOG18 and 250 764 for GDR2. The difference of a factor ~ 2 between the two catalogues in the pre-selected fraction is caused by imperfect modelling of the disc stellar population or inaccurate estimation of observational errors in GOG18. Observational errors are provided only for end-of-mission results in GOG18, while GDR2 is based on data collected during the first 2 yr of the *Gaia* mission, so we have corrected the GOG18 errors as in section 3.1 of PM19 but this correction may be inaccurate. Incompleteness of the GDR2 catalogue in areas with lower than average exposure or high stellar density and inaccurate modelling of dust extinction in GOG18 may be other reasons for the difference of the simulated and real catalogues. Cut 5 has again a relatively small impact and removes more stars in the vicinity of NGC 3201 in GDR2 than in GOG18 because the latter does not include globular clusters.

Cuts 6 and 7 are applied only after the best fit to the stream has been computed, to obtain a list of the most likely candidate stream members. Cut 6 involves an accurate kine-

Table 2. Total number of stars in GOG18 and GDR2 and number that pass each cut. For cuts 6 and 7, the number of stars left is shown divided in six sky regions, where the tidal tail is seen under different foreground conditions, and a different value of the threshold χ_{sel} defined in section 3.4 is used, specified in units of $\text{yr}^3 \text{deg}^{-2} \text{pc}^{-1} \text{mas}^{-3}$. Numbers in parentheses for GOG18 indicate the expected number of stars if GOG18 had the same number of pre-selected stars as GDR2 in each region. Note that cut 7 is not used to obtain the best-fitting tidal stream model, but only for the final selection of candidate stream members. The number of selected stars combining all six regions is shown at the bottom.

Pre-selection cut	GOG18	GDR2
All catalogue	1510 398 719	1692 919 135
(1) - (2)	1490 962 149	1313 216 777
(4)	492 983	250 764
(5)	486 664	218 065
Region (i) Disc foreground 1		
(6) $\chi_{\text{sel}} = 4.9 \times 10^{-2}$	2 (1)	18
(7)	1 (0)	12
Region (ii) Disc foreground 2		
(6) $\chi_{\text{sel}} = 7 \times 10^{-3}$	1 (0)	14
(7)	1 (0)	8
Region (iii) Stream		
(6) $\chi_{\text{sel}} = 5 \times 10^{-3}$	10 (4)	55
(7)	8 (4)	51
Region (iv) Dust		
(6) $\chi_{\text{sel}} = 5.38 \times 10^{-4}$	1 (0)	7
(7)	0 (0)	6
Region (v) Globular Cluster		
(6) $\chi_{\text{sel}} = 2.9 \times 10^{-3}$	11 (5)	75
(7)	2 (1)	71
Region (vi) Disc foreground 3		
(6) $\chi_{\text{sel}} = 6 \times 10^{-3}$	3 (1)	28
(7)	2 (1)	22
All regions combined		
(6)	28 (13)	197
(7)	14 (6)	170

matic consistency with the best-fitting stream model, and cut 7 requires photometric compatibility with the progenitor cluster H-R diagram, and will be discussed in detail in section 3.4.

The pre-selected stars, passing cuts 1 to 5, are shown in the top panel of Figure 4 as grey dots, in an equatorial coordinates sky map with the Galactic latitude $b = \pm 15$ deg shown as dashed lines, and the position of NGC 3201 shown as a blue dot. These pre-selected stars follow roughly the cluster orbit only because we have required this in cut 4 when selecting stars consistent with a bundle of orbits around that of NGC 3201, including uncertainties in the distance and kinematic measurements and in the Galactic potential model. However, the black dots in the top panel include the additional cut 7 (imposing a consistent color with the NGC 3201 H-R diagram at the distance of the stream model, see section 3.4). The narrow band of these black dots seen in the range $70 \lesssim \alpha \lesssim 100$ degrees is already a visual evidence of the presence of the stream.

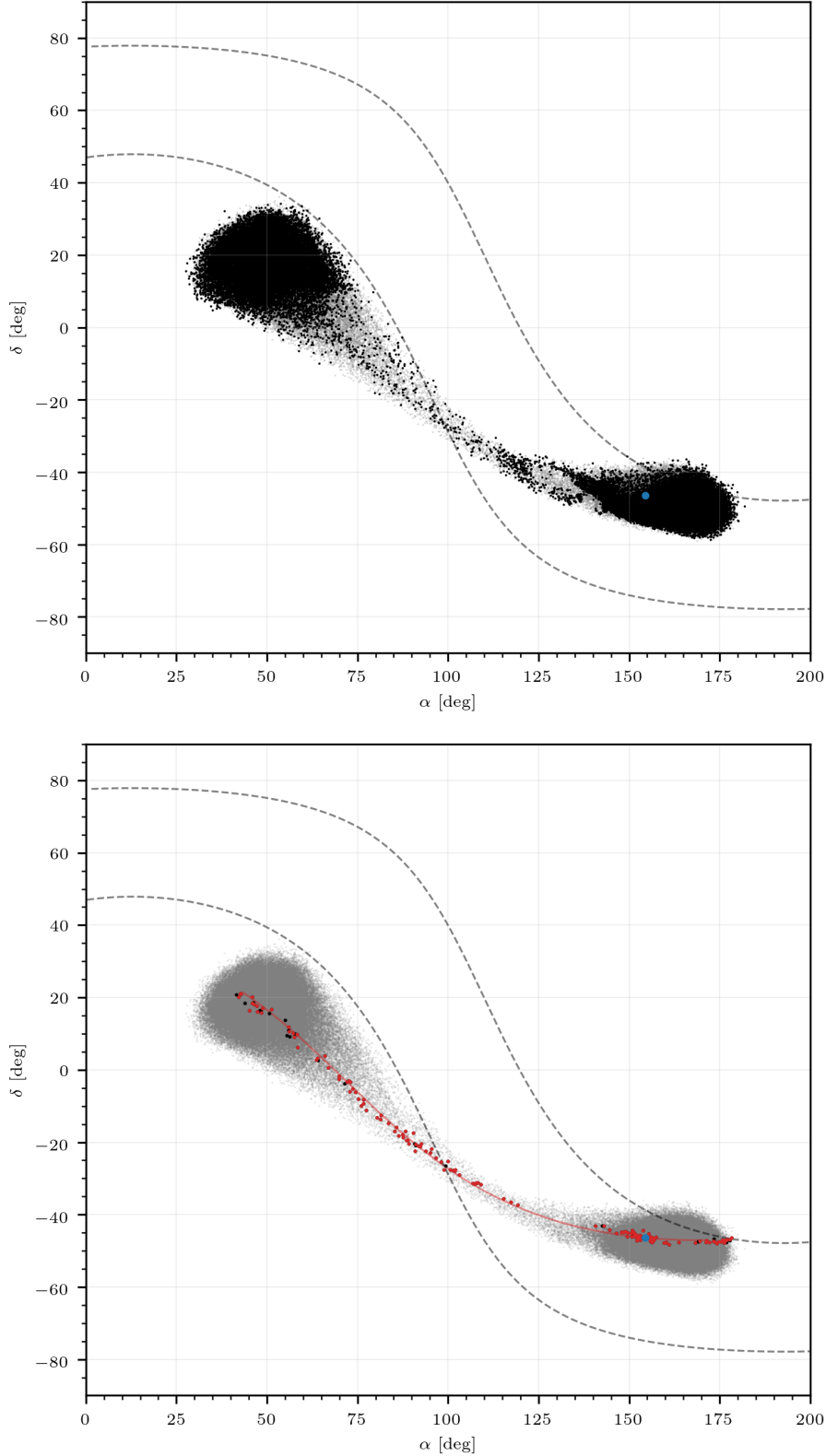


Figure 4. *Top:* Sky map in equatorial coordinates of the pre-selected stars from GDR2 passing cuts 1, 2, 4, 5 (grey dots), which are the stars that are judged to be roughly compatible with stream membership before the fit is done, and are used to obtain the final fit. Stars that are also compatible with the H-R diagram of NGC 3201 (passing cut 7) are highlighted in black. An elongated overdensity in the range $\alpha \sim [75-100]$ deg and an obscured region by dust in $\alpha \sim [120-145]$ deg can be seen, which is much sharper and clearer for stars passing cut 7, indicating the presence of the stream. The blue dot is the present cluster position, and the grey lines indicate Galactic latitude $b = \pm 15$ deg. *Bottom:* Final selection of GDR2 stars. The grey small dots are the same as in the top panel, black dots are stars compatible with the density model of the best-fitting stellar stream (stars passing cut 6 with our chosen values of χ_{sel} in different regions), and red dots are stars that are also compatible with the NGC 3201 H-R diagram (passing cut 7). The red line is the best-fitting orbit of NGC 3201 from -60 to $+10$ Myr from the present time.

3.2 Best fit to tidal stream from GDR2 kinematic data

We now apply the method of maximum likelihood to compute the best-fitting parameters of the stream model, varying both orbital parameters of NGC 3201 with the prior of the distance, radial velocity and proper motion observational determinations, and parameters for the Galactic halo determining the gravitational potential. The method we use is fully described in PM19 and is based on an approximate calculation of a likelihood function, computed from a stellar density of the tidal stream inferred from our stream simulation, and from a model distribution function of the foreground stars belonging to the general Milky Way stellar populations. As explained in section 2.5.1 of PM19, the simulation that is used to compute a model of the stream stellar distribution is performed by following the trajectory of stars that are initially in orbits with a significant escaping probability (obeying equation 21 in PM19), derived from a tidal radius $r_t = R_c [M_{gc}/(3M_t)]^{1/3}$, where R_c is a characteristic orbital radius of the cluster, $M_t = 5.2 \times 10^{11} M_\odot$ is the total Galaxy mass (this was written as M in equations 19 and 20 of PM19), and M_{gc} is the globular cluster mass given in Table 1. The true tidal radius is somewhat smaller than r_t because only the Galaxy mass interior to R_c counts for generating the tidal stress on the cluster, but in practice we adjust R_c so that fewer than 30 per cent of the stars that escape are missed because of not including them in our fast simulations that follow only stars with a high escape probability. We have chosen on this basis $R_c = 15$ kpc for NGC 3201 in this paper.

We do not apply this method using the entire *Gaia* stellar catalogue, which would be prohibitively expensive computationally, but we use only the pre-selected stars to compute our likelihood function. This essentially neglects the possibility that any stars outside our pre-selected sample might be stream members. The free parameters we use and their best-fitting results are listed in Table 3: the fraction of stars τ in the stellar stream, parameters of the halo density profile (ρ_{0dh} , a_{1dh} , a_{2dh} , and β_{dh}), and the heliocentric distance, radial velocity and proper motions of the globular cluster. Gaussian priors from the observational results listed in Table 1 are used for the cluster present phase-space coordinates, while the remaining parameters are given uniform priors wide enough to be unimportant for the results. Errors listed in Table 3 are from the diagonal elements of a full covariance matrix of all the free parameters, computed from the second derivatives of the posterior function. A few other derived parameters for the NGC 3201 orbit, and statistical measures defined in PM19, are also included in Table 3.

Our results can be described according to the following three points:

(i) A tidal stream of NGC 3201 is detected at a very high confidence level. This is inferred by maximizing the likelihood function, which essentially corresponds to maximizing the overlap of the stream phase-space distribution model with the stellar distribution in our pre-selected data. The value of $\tau \sim 3 \times 10^{-4}$ we find for our best fit, which is the fraction of stars in our pre-selected sample that belong to the stream if the best-fitting model is correct, has a relatively error of only 12 per cent, so it is greater than zero with a very high statistical significance. Note that this number does not have a useful physical interpretation because it depends

Table 3. Best-fit parameters obtained for the NGC 3201 orbit and the Galactic dark halo, using the GDR2 pre-selected data.

Statistical parameters		
Λ		364.61
τ		$(2.74 \pm 0.35) \times 10^{-4}$
Q		17.95
Best-fitting kinematics of NGC 3201		
r_h	(kpc)	4.79 ± 0.05
v_r	(km s ⁻¹)	494.304 ± 0.14
μ_δ	(mas yr ⁻¹)	-1.9859 ± 0.0014
μ_α	(mas yr ⁻¹)	12.1048 ± 0.0022
Dark halo best-fitting parameters		
ρ_{0dh}	(M _⊙ kpc ⁻³)	$(6.87 \pm 0.09) \times 10^6$
a_{1dh}	(kpc)	18.67 ± 0.27
a_{3dh}	(kpc)	16.29 ± 0.25
β_{dh}	-	2.845 ± 0.035
q	-	0.87 ± 0.02
$q\phi$	-	0.94 ± 0.01
c_{200}	-	9.14 ± 0.2
r_{200}	(kpc)	202.2 ± 5.2
M_{200}	(M _⊙)	$(9.71 \pm 0.75) \times 10^{11}$
Derived NGC 3201 orbital parameters		
r_{peri}	(kpc)	7.67 ± 0.03
r_{apo}	(kpc)	37.62 ± 1.41
L_z	(km s ⁻¹ kpc)	2728.8 ± 18.4

on our pre-selection method, and also on the complex details of the selection of the *Gaia* catalogue. In addition, the value of the statistic Λ indicates the confidence level at which the presence of the stream is detected, as explained in PM19 (Section 2.1). When $\Lambda > 6.6$, the existence of the stream is confirmed at the 99 per cent confidence level compared to the null hypothesis that no stream is present. The large value of Λ implies a very high detection statistical significance.

(ii) The best-fitting orbit of NGC 3201 matching the detected stream is remarkably close to the orbit that is derived exclusively from the independent observational determinations of the cluster phase-space coordinates. The statistical parameter Q quantifies the deviation of the best-fitting present phase-space coordinates of NGC 3201 from the observational determinations in Table 1. Its expected value is the number of parameters of the globular cluster orbit that are fitted (in this case 4, as given in Table 3). The larger obtained value $Q \simeq 18$ is mostly due to the deviation of the best-fitting from the observed proper motion along right ascension, a 4.3σ deviation. We note that this deviation, while significant compared to the small statistical measurement errors of the GDR2 proper motion of the globular cluster, are actually less than 0.2 per cent of the proper motion. This small deviation may be caused by underestimates of errors provided by [Gaia Collaboration et al. \(2018\)](#) for globular cluster proper motions, obtained by averaging measurements of a large number of member stars. Both [Vasiliev \(2019\)](#) and [Baumgardt et al. \(2019\)](#) provide bigger uncertainties compatible with our results.

(iii) In our Galactic potential model where only halo parameters are allowed to vary, our best-fit result for these parameters (listed in Table 3) has relatively small errors, and is remarkably close to our best-fitting M68 stream model from

PM19 (with values listed in Table 1). In particular, the axis ratio of the halo mass density distribution $q = 0.87$ has an error of only 2 per cent, and is in very good agreement from the two streams. However, these small errors are of course the result of assuming a fixed model for the disc and bulge parameters. If these are allowed to vary, parameter degeneracies arise which are expected to increase the error in the halo parameters by a large factor. In addition, the computation of the uncertainties by the second derivative of the likelihood function underestimates the errors of the free parameters when the posterior function is not smooth over the entire range of possible parameter values. Mainly, this occurs for the halo parameters.

3.3 Visualization of stream including photometric selection

Apart from obtaining the best fit to the stream using the kinematic data and noting the large value of Λ in Table 3, there is an alternative way to test the reality of the stream: we can search for stars with photometry that is compatible with the H-R diagram of NGC 3201, assuming that they are stream members and are at the distance predicted by the stream model. These stars should be distributed along a narrow region of phase-space corresponding to the stream when compared to the whole pre-selected sample.

We define a seventh cut (7) that selects stars consistent with the H-R diagram of the globular cluster NGC 3201, obtained directly from the GDR2 catalogue as described in Appendix A. The method is the same as that described in PM19 (section 3.5 and Appendix D), which basically defines a density model in the H-R diagram based on the cluster member stars, and then selects stream stars with a position in the H-R diagram above a threshold density (we use in this paper a threshold $P_{\text{CR}} \gtrsim 0.035 \text{ mag}^{-2}$, as defined in equation D5 of PM19). An important difference from PM19 is, however, introduced: we take into account dust extinction, which in this case is important because the cluster is located close to the Galactic plane in a region of moderately high extinction, and the stream is also affected by varying amounts of extinction over its long extent. The corrections applied to stars to both the magnitude and color for dust extinction and reddening are from Schlafly & Finkbeiner (2011), known as the SF dust extinction map model, and is described in detail in Appendix B. Note that this dust correction is obtained from the SF model assuming that all the dust is foreground to the stars, an assumption that is valid in most cases for stars with low *Gaia* parallax except when looking at very low Galactic latitude (in which case extinction is very high anyway).

Among all the pre-selected stars shown as grey dots in Figure 4, those that are in addition compatible with the NGC 3201 H-R diagram (cut 7) are shown as black dots of larger size in the top panel. The large blue dot is the present position of NGC 3201. An elongated overdensity which is narrower than the whole pre-selected sample is clear in the range $70 \lesssim \alpha \lesssim 100 \text{ deg}$. We note that the region very close to the Galactic plane has very few stars that pass this cut 7. The reason is the very large extinction present in this region.

The stream and selected stars are better visualized by plotting these maps in rotated spherical coordinates, where the angle ϕ_1 varies along a major circle that approximately follows the stellar stream, and the angle ϕ_2 is a polar an-

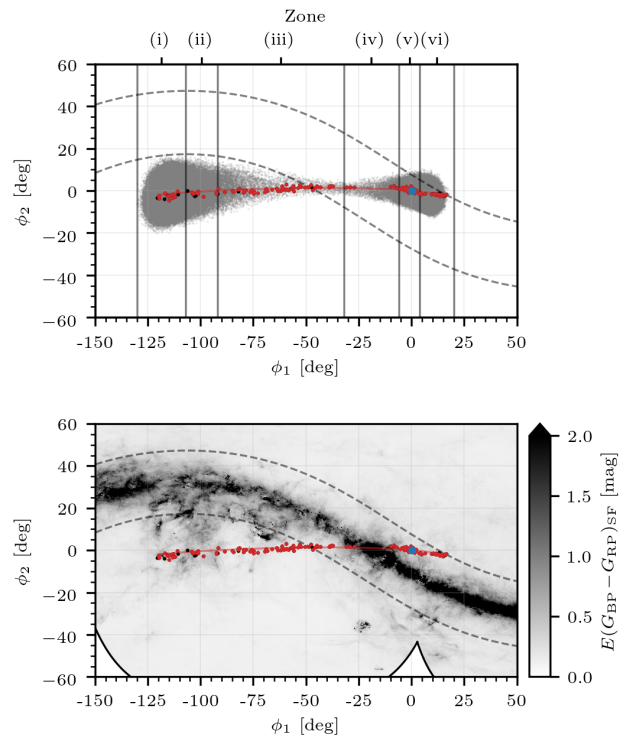


Figure 5. Same as bottom panel of Figure 4, expressed in a stream coordinate system with the ϕ_1 axis following the cluster orbit, as specified in Appendix D. *Top:* The solid vertical lines mark selection zone limits. *Bottom:* Colour excess of the $G_{\text{BP}} - G_{\text{RP}}$ colour index from the SF extinction map (Schlafly & Finkbeiner 2011), a recalibrated version of the SFD extinction map (Schlegel et al. 1998). Only the best-fitting stream candidate member stars after cut (6) are shown here.

gle from the axis perpendicular to this major circle. The bottom panel of Figure 4 shows stars that pass not only cut 7, but also cut 6 which requires kinematic consistency with the best-fitting stream model (described in detail in the next subsection). This is replotted in the stream coordinates (ϕ_1, ϕ_2) in Figure 5 in the top panel. The bottom panel of Figure 5 adds the dust extinction map of the SF model (Schlafly & Finkbeiner 2011). We can see that the region of the stream with an absence of stars compatible with all our cuts coincides with the region of highest dust extinction. The globular cluster NGC 3201 is seen at a moderately low, northern Galactic latitude, where dust extinction is close to 1 magnitude, and the trailing arm is the one that passes closest to the Solar System and is therefore most visible to us. This trailing arm crosses the Galactic disc and reappears on the southern Galactic hemisphere, where most of the stream candidates in the GDR2 catalogue can be identified.

3.4 Final stream star selection including photometry

The final procedure in our study of the tidal stream is to select a list of stars that are most likely to be stream members, using both the stellar density of the stream model that gives the maximum likelihood, and the photometric condition of consistency with the cluster H-R diagram. First, cut 6 selects the stars with kinematic variables that are compatible

with the best-fitting stream model, and then cut 7 restricts our final list to stars compatible with the H-R diagram.

The stream phase-space density model is constructed as in PM19, similar to the way we evaluate the likelihood function, from the superposition of several Gaussian distributions along the stream. We compute the phase-space density at the phase-space position of each of the pre-selected stars for the best-fitting density model, convolving it with the observational errors of the phase-space coordinates, and we select stars with a value of this convolved phase-space density above a threshold χ_{sel} , which is expressed in units of $\text{yr}^3 \text{deg}^{-2} \text{pc}^{-1} \text{mas}^{-3}$. The procedure is also done with the simulated stars in the GOG18 catalogue, and the threshold is chosen in each zone so that a small number of GOG18 stars are selected as stream members (this small number obviously represents our noise level of false candidates because there are no streams in the GOG18 simulation).

In practice, the stream we are analysing is very long and the different regions of the sky over which it is projected have very different levels of foreground contamination. To optimize our stream candidate list, we divide the sky into six different zones and use a different value of χ_{sel} in each one. We set the zone limits in the stream coordinate ϕ_1 , defined to be the angle along a major circle that is approximately followed by the stream. The transformation from equatorial to these stream coordinates is given in Appendix D. The six regions, shown in the top panel of Figure 5, are defined as follows:

- (i) *Disc foreground 1*: $-130 \leq \phi_1 < -107$ (deg)
- (ii) *Disc foreground 2*: $-107 \leq \phi_1 < -92$ (deg)
- (iii) *Clean stream*: $-92 \leq \phi_1 < -32$ (deg)
- (iv) *High dust*: $-32 \leq \phi_1 < -6$ (deg)
- (v) *Globular cluster*: $-6 \leq \phi_1 < 4$ (deg)
- (vi) *Disc foreground 3*: $4 \leq \phi_1 \leq 20$ (deg)

We list in Table 2 the number of stars of the GOG18 and GDR2 catalogues that pass cuts 6 and 7, and the value of the selection threshold χ_{sel} we choose for each zone.

In zones (i), (ii), and (vi), the density of foreground stars is very high because the proper motions and parallaxes of most disc stars are small and cannot be distinguished from the stream stars. This makes our cuts less effective at reducing the number of stars in our pre-selected sample. Taking these three zones together, we select 60 stars from GDR2 that pass cut 6, while only six are found by chance in GOG18 with the same values of χ_{sel} . This suggests most of the 60 stars found in this zone are real stream members, even before applying our cut 7. Actually, the number of six stars found in GOG18 in these three zones is an overestimate of the number of false candidates we should expect in GDR2, because the number of stars that are pre-selected in GOG18 is larger than in GDR2 (as seen in Table 2 in the total number of pre-selected stars after cut 5). A more reasonable estimate of the expected number of false candidates in GDR2 is obtained by correcting the number found in GOG18 according to the ratio of pre-selected stars after cut 5 in GOG18 and GDR2 in each of our six zones. This corrected estimate

is written in parenthesis after the GOG18 number in each zone. For these three zones, the expected number of false candidates is reduced to 2 or 3. When applying in addition cut 7, the stream candidates are reduced to 42. In GOG18, the noise candidates are not reduced very much by cut 7 because most of the contaminating disc stars in these regions have colours that happen to be compatible with the NGC 3201 H-R diagram when the model stream distance is assumed.

Zone (iv) is highly obscured by dust (see Figure 5). Only seven stars are selected, of which six are compatible with the cluster H-R diagram. These stars are actually all located at the edges of zone (iv), where the dust extinction is not so high, and we therefore think they are most likely true stream members.

Zone (v) corresponds to the vicinity of NGC 3201. We select 75 stars, of which 71 are compatible with the cluster H-R diagram. In contrast, in GOG18 only 11 stars pass cut 6, of which only 2 pass cut 7, indicating that most of our final 71 stars from this zone are truly associated with the cluster. Our cut 5 removes stars only within an angle of 1.5 deg from the centre of NGC 3201, and there may still be some cluster member stars outside this angle that are bound to the cluster; in fact, the 71 stars in zone (v) we include in our final selection are rather concentrated towards the cluster. It is in general ambiguous to separate stars that are still bound from those that are already considered as stream members.

Finally, zone (iii) is the cleanest because it contains the part of the stream that is closest to us, located at ~ 3.2 kpc from the Sun, with proper motions that are larger than those of most foreground stars. Dust extinction is also relatively low. To analyze the selection in this particularly favourable zone more carefully, Figure 6 shows the number of selected stars, N_{sel} , as a function of the selection threshold for this zone. The solid black line is the number of GDR2 stars selected for each threshold value, and the red one shows the number that are also compatible with the NGC 3201 H-R diagram. The two lines coincide up to $N_{\text{sel}} \sim 100$, whereas at larger numbers (or lower χ_{sel}) we start having many stars passing cut 6 which do not pass cut 7. This implies that for $N_{\text{sel}} \lesssim 100$, most selected stars should be true members. Dashed lines are the same for GOG18 stars. The shaded area below the dashed stars indicates the range by which the number of stars found in GOG18 drops because of the correction applied for the fact that GOG18 contains more stars than are detected in GDR2 in our pre-selected sample. As χ_{sel} is dropped, the number of selected stars in GOG18 rises to an increasing fraction of the ones found in GDR2. For our chosen value of χ_{sel} in zone (iii), we select 55 stars of which 51 also pass cut 7, expecting a number of wrongly selected stars of only ~ 4 .

Our final selection over all regions contains 170 stars compatible with our best-fitting stream model and the cluster H-R diagram. Our GOG18 estimate of the foreground contamination predicts that the number of false members in this list is probably as low as ~ 6 . These stars are plotted as red dots in the bottom panel of Figure 4 and in Figure 5, with black dots being for stars that pass only cut 6 but not cut 7. We also show the best-fitting orbit of NGC 3201 as a red solid line.

Figure 7 shows other variables for these same stars: par-

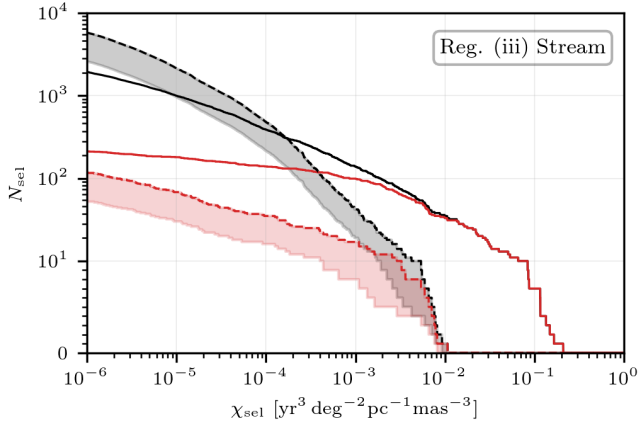


Figure 6. Number of selected stars N_{sel} in zone (iii) as a function of the selection threshold χ_{sel} . *Black solid line*: number of GDR2 stars compatible with the best-fitting stream model, passing cut 6. *Red solid line* number of stars also compatible with NGC 3201 H-R diagram (cut 7). *Dashed lines*: same quantities for GOG18 stars. Shaded areas mark the reduction due to correcting for the larger number of pre-selected stars in GOG18 than in GDR2.

allax versus declination in the top panel, proper motions in the middle panel, and the H-R diagram in the bottom panel (with cluster members as small grey dots). Observational errors are indicated as thin black lines. The top panel shows that the parallax is not a very useful discriminant because the distance to the stream is too large for present *Gaia* uncertainties, but is nevertheless of some use and fits well the expected orbit. Proper motions are the most valuable information when detecting and modelling the stream. We note that, remarkably, using only the kinematic selection for stream members (up to cut 6, which are both the red and black dots), and inferring their absolute magnitude from the stream model distance and correcting for dust, we reproduce the H-R diagram of the cluster notably well.

The list of our final 170 stream member candidates is in Appendix C, with their measured coordinates, parallax and proper motion, colour index $G_{\text{BP}} - G_{\text{RP}}$, and G -band magnitude. Only one star has a *Gaia* radial velocity in GDR2 of 499.29 km s^{-1} , which we find to be in agreement with the orbital radial velocity prediction of 498.75 km s^{-1} . We have checked the RAVE DR5 (Kunder et al. 2017) and the LAMOST DR4 (Luo et al. 2015) catalogues, and have not found any matches to this list.

4 CONCLUSIONS

The method presented in PM19 is applied to search for a tidal stream associated with the globular cluster NGC 3201. This method identifies the stellar stream by statistically detecting star overdensities in a sample of observational data with respect to a phase-space density model of the Milky Way. For the best-fitting location of the globular cluster and the parameters of the gravitational potential, we construct a density model of the stream and select the stars with the highest intersection. Finally, we present as a final selection the stars that are also compatible with the H-R diagram of the progenitor cluster.

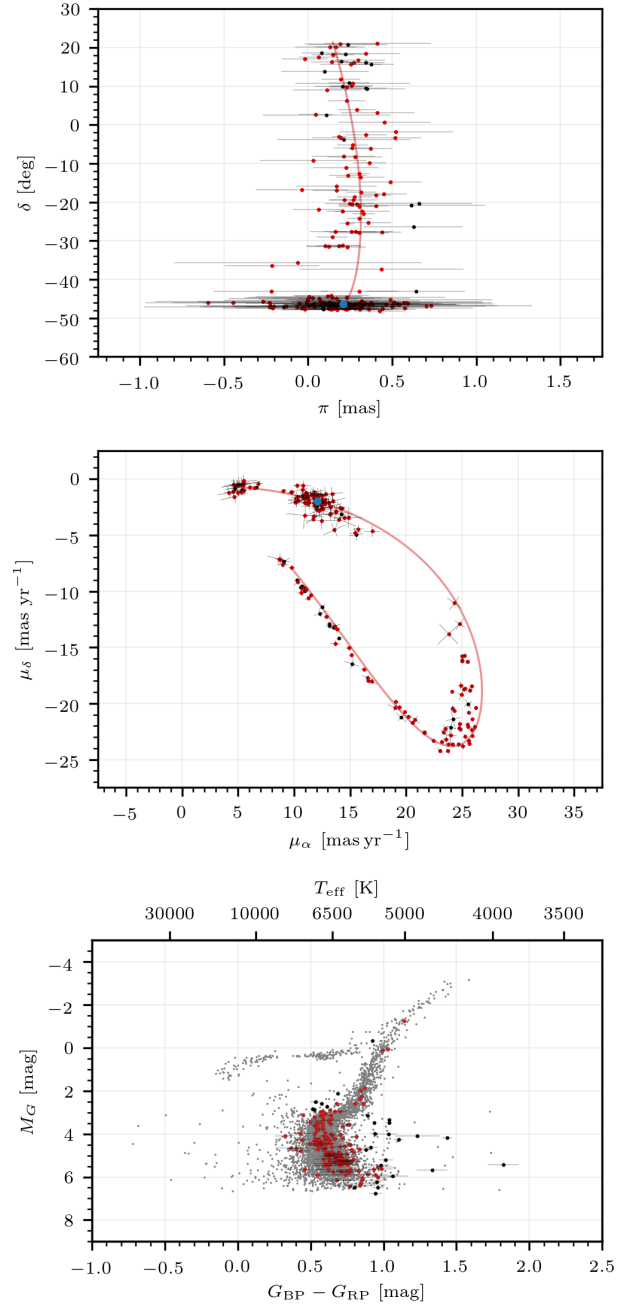


Figure 7. Parallax versus declination (top), proper motions (middle), and dust-corrected $G_{\text{BP}} - G_{\text{RP}}$ colour versus absolute G -band magnitude (bottom) for the 197 stars in our final selection after cut 6, with 170 of them passing also cut 7 shown in red, and the remaining 27 in black. Thin black lines are observational errors. Small grey dots in bottom panel are stars in NGC 3201.

We detect a total of 170 stars candidates along the leading and the trailing arm of the stellar stream, extending over ~ 140 deg on the sky, from 40 to 180 deg in the Southern Galactic hemisphere, following an orbit of $L_z = 2728.8 \pm 18.4 \text{ km s}^{-1} \text{ kpc}$. The clearest section of the stream spans from 70 to 105 deg, close to the Galactic disc, at about 3.2 kpc from the Sun. This section coincides with the known stellar stream Gjörl discovered by Ibata et al. (2019) using the method Streamfinder (Malhan & Ibata 2018; Malhan et al.

2018a), which spans from 70 to 90 deg in the Southern Galactic hemisphere, at 3.38 ± 0.1 kpc from the Sun, following an orbit of $L_z = 2721 \pm 159$ km s⁻¹ kpc. This association based on *Gaia* phase-space, colours, and magnitudes together with the chemical tagging of stars in the stream to NGC 3201 (Hansen et al. 2020), proves that Gjöll is a section of the trailing tail of NGC 3201.

Our best-fitting parameters are consistent with the observations of NGC 3201 and provide a consistent model of the Milky Way. Even so, our computation underestimates the uncertainties of the halo parameters and cannot be considered representative of our current understanding of the density and potential of the Galaxy. In a future study, we will be using a combination of several streams to study the constraints that can be set on the Milky Way potential, especially the shape of the dark matter halo, by fitting models with sufficient parametric freedom on all the Galactic components to the observed data on all the stellar streams. Our success in detecting this stream opens the possibility to detect many more fainter stellar streams associated with globular clusters, as the *Gaia* data improve and the separation from foreground stars becomes more efficient.

ACKNOWLEDGEMENTS

We would like to thank Holger Baumgardt for useful comments about the mass of NGC 3201. This work has been supported by Spanish grants MDM-2014-0369 and CEX2019-000918-M, for the Unit of Excellence Maria de Maeztu award to the ICCUB. Use of data from the European Space Agency (ESA) mission *Gaia* (<https://www.cosmos.esa.int/gaia>) was made, processed by the *Gaia* Data Processing and Analysis Consortium (DPAC, <https://www.cosmos.esa.int/web/gaia/dpac/consortium>). Funding for the DPAC has been provided by national institutions, in particular, the institutions participating in the *Gaia* Multilateral Agreement.

DATA AVAILABILITY

The data underlying this article are available in the article and in its online supplementary material.

REFERENCES

- Anguiano B., et al., 2016, *MNRAS*, **457**, 2078
 Baumgardt H., Hilker M., Sollima A., Bellini A., 2019, *MNRAS*, **482**, 5138
 Bianchini P., Ibata R., Famaey B., 2019, *ApJ*, **887**, L12
 Chen C. W., Chen W. P., 2010, *ApJ*, **721**, 1790
 Gaia Collaboration et al., 2018, *A&A*, **616**, A12
 Grillmair C. J., 2019, *ApJ*, **884**, 174
 Grillmair C. J., Carlin J. L., 2016, in Newberg H. J., Carlin J. L., eds, *Astrophysics and Space Science Library Vol. 420, Tidal Streams in the Local Group and Beyond*. p. 87 ([arXiv:1603.08936](https://arxiv.org/abs/1603.08936)), doi:10.1007/978-3-319-19336-6_4
 Hansen T. T., Riley A. H., Strigari L. E., Marshall J. L., Ferguson P. S., Zepeda J., Sneden C., 2020, *ApJ*, **901**, 23
 Harris W. E., 1996, *AJ*, **112**, 1487
 Harris W. E., 2010, arXiv e-prints, p. [arXiv:1012.3224](https://arxiv.org/abs/1012.3224)
 Ibata R. A., Malhan K., Martin N. F., 2019, *ApJ*, **872**, 152
 Jordi C., et al., 2010, *A&A*, **523**, A48
 Kunder A., et al., 2014, *A&A*, **572**, A30
 Kunder A., et al., 2017, *AJ*, **153**, 75
 Kundu R., Minniti D., Singh H. P., 2019, *MNRAS*, **483**, 1737
 Luo A. L., et al., 2015, *Research in Astronomy and Astrophysics*, **15**, 1095
 Luri X., et al., 2014, *A&A*, **566**, A119
 Malhan K., Ibata R. A., 2018, *MNRAS*, **477**, 4063
 Malhan K., Ibata R. A., Goldman B., Martin N. F., Magnier E., Chambers K., 2018a, *MNRAS*, **478**, 3862
 Malhan K., Ibata R. A., Martin N. F., 2018b, *MNRAS*, **481**, 3442
 Mateu C., Cooper A. P., Font A. S., Aguilar L., Frenk C., Cole S., Wang W., McCarthy I. G., 2017, *MNRAS*, **469**, 721
 Navarro J. F., Frenk C. S., White S. D. M., 1996, *ApJ*, **462**, 563
 Palau C. G., Miralda-Escudé J., 2019, *MNRAS*, **488**, 1535
 Sanderson R. E., Helmi A., Hogg D. W., 2015, *ApJ*, **801**, 98
 Schlafly E. F., Finkbeiner D. P., 2011, *ApJ*, **737**, 103
 Schlegel D. J., Finkbeiner D. P., Davis M., 1998, *ApJ*, **500**, 525
 Shipp N., et al., 2018, *ApJ*, **862**, 114
 Sollima A., Baumgardt H., 2017, *MNRAS*, **471**, 3668
 Vasiliev E., 2019, *MNRAS*, **484**, 2832

APPENDIX A: COLOUR-MAGNITUDE DIAGRAM OF NGC 3201 FROM GDR2

We reproduce here the ADQL query we have used to obtain the photometry of all GDR2 stars in the G , G_{BP} , and G_{RP} passbands in a circle of radius 0.14 deg centred on NGC 3201, which yields 7064 stars:

```

1 SELECT bp_rp, phot_g_mean_mag,
   phot_bp_mean_flux,
   phot_bp_mean_flux_error,
   phot_rp_mean_flux,
   phot_rp_mean_flux_error,
   phot_g_mean_flux,
   phot_g_mean_flux_error
2 FROM gdr2.gaia_source
3 WHERE 1 = CONTAINS( POINT('ICRS', ra,
   dec), CIRCLE('ICRS', 154.3987,
   -46.4125, 0.14) )
4 AND parallax BETWEEN -1.6 AND 1.4
5 AND SQRT((pmra-8.3344)*(pmra-8.3344) + (
   pmdec+1.9895)*(pmdec+1.9895)) <= 0.7
6 AND bp_rp IS NOT NULL;
```

Host server: <https://gaia.aip.de/>
 Description of the `gaia_source` table:
https://gea.esac.esa.int/archive/documentation/GDR2/Gaia_archive/chap_datamodel/sec_dm_main_tables/ssec_dm_gaia_source.html

APPENDIX B: DUST EXTINCTION CORRECTION

To select stars that are consistent with the H-R diagram of NGC 3201, the $G_{BP}-G_{RP}$ colour index and the G -band magnitude observed by *Gaia* need to be corrected for the effects of dust extinction, both for the cluster stars and the candidate stream stars. In general, for any observed colour index M' , the corrected colour index M is computed by subtracting the colour excess E_M ,

$$M = M' - E_M. \quad (\text{B1})$$

We use the colour excess E_{B-V} for $B-V$ colour predicted by the Galactic dust model of [Schlafly & Finkbeiner \(2011\)](#), known as the SF model. This is the same as the colour excess model of $B-V$ from [Schlegel et al. \(1998\)](#) reduced by a factor 0.86. The $B-V$ colour of stars can be related to the *Gaia* colour $G_{BP}-G_{RP}$, for most common stellar metallicities and gravities, using the approximate expression of [Jordi et al. \(2010\)](#), from their Table 3:

$$G_{BP}-G_{RP} = 0.0981 + 1.429(B-V) - 0.0269(B-V)^2 + 0.0061(B-V)^3. \quad (\text{B2})$$

We also follow the approximation of [Jordi et al. \(2010\)](#) that the dust extinction colour excess runs nearly parallel to this colour-colour relation. Neglecting the small coefficients of the second- and third-order terms in $B-V$, we can use the simple approximation

$$E_{G_{BP}-G_{RP}} = 1.429 E_{B-V}. \quad (\text{B3})$$

The extinction correction in the G -band magnitude A_G can be approximately expressed in terms of the colour excess

$G_{BP}-G_{RP}$. We use the expression calibrated at a typical dust extinction $A_{\lambda=550\text{ nm}} = 1$ mag, given in table 13 of [Jordi et al. \(2010\)](#):

$$A_G = 1.98 E_{G_{BP}-G_{RP}}. \quad (\text{B4})$$

APPENDIX C: FINAL CANDIDATE STREAM MEMBER STARS

The selected stars from GDR2 catalogue after all our cuts from 1 to 7 are applied, which are our final list of best candidate stream members, are listed in Table C1. Only one star in this list, star number 144, has a radial velocity:

N	source_id	v_r (km s ⁻¹)	ϵ_{v_r} (km s ⁻¹)
144	5365576065920333440	499.29	1.29

APPENDIX D: DEFINITION OF STREAM COORDINATES

We have defined stream spherical coordinates on the sky by defining the angle ϕ_1 along a major circle that approximately contains the stream, and ϕ_2 to be the polar angle from the axis perpendicular to this major circle. An approximate adjustment to these coordinates by eye has resulted in the following coordinate transformation matrix from the usual equatorial coordinates (α, δ) :

$$\begin{pmatrix} \cos(\phi_2) \cos(\phi_1) \\ \cos(\phi_2) \sin(\phi_1) \\ \sin(\phi_2) \end{pmatrix} = M \times \begin{pmatrix} \cos(\delta) \cos(\alpha) \\ \cos(\delta) \sin(\alpha) \\ \sin(\delta) \end{pmatrix}, \quad (\text{D1})$$

where the transformation matrix is:

$$M = \begin{pmatrix} -0.6209 & 0.2992 & -0.7245 \\ -0.4004 & -0.9157 & -0.0350 \\ -0.6739 & 0.2684 & 0.6883 \end{pmatrix}. \quad (\text{D2})$$

This paper has been typeset from a \LaTeX file prepared by the author.

Table C1. List of candidate stream member stars from the GDR2 catalogue, having passed all our 7 cuts. They are compatible with the best-fitting phase-space density model of the tidal stream of NGC 3201 and its H-R diagram from GDR2 after dust extinction correction.

N	source_id	π (mas)	δ (deg)	α (deg)	μ_δ (mas yr ⁻¹)	$\mu_{\alpha*}$ (mas yr ⁻¹)	$G_{BP}-G_{RP}$ (mag)	G (mag)	χ_{sel} (yr ³ deg ⁻² pc ⁻¹ mas ⁻³)
1	85111820717084288	0.1651	+20.1781	42.2098	-7.9041	9.1652	0.8645	17.6426	8.1257E-02
2	85463664437883264	0.4112	+21.1340	42.5690	-7.1268	8.0718	1.1816	18.7109	5.3786E-02
3	85259674966320512	0.1913	+20.9929	42.8676	-7.1869	8.2032	1.2189	18.1123	2.9994E-01
4	34258896831609984	0.1405	+16.3693	45.1634	-9.6897	10.4887	0.9566	17.5377	5.3842E-02
5	35721109857582464	0.3439	+18.4065	45.9215	-9.1765	9.7779	1.0528	18.0348	6.4986E-02
6	60185926474933632	0.1295	+20.1024	46.0006	-7.6207	8.4273	0.8544	18.1997	5.3196E-02
7	34901557082616576	0.1467	+18.1273	46.4329	-9.8855	10.5074	0.7827	17.6309	6.2463E-02
8	58640189220402432	0.0641	+17.6070	47.2249	-9.7492	10.2046	0.8839	17.2243	2.0020E-01
9	31456447850977536	0.2736	+16.1339	47.4120	-9.7023	10.2854	1.1301	16.8443	2.1423E-01
10	31185242140302080	0.2541	+15.7169	48.4324	-10.1471	10.2482	0.9355	18.2953	8.7513E-02
11	55510772969455232	-0.0189	+17.0169	48.7138	-10.3461	10.9882	1.1011	16.5356	7.4714E-02
12	54919579310541568	0.2956	+16.7824	51.1901	-10.6029	10.7765	0.8089	17.7362	6.3037E-02
13	37334471374125696	0.1933	+11.8852	55.9878	-12.2495	12.5768	1.3554	17.3445	4.3200E-02
14	36354359837010816	0.2640	+10.6748	56.0746	-13.0978	13.3644	0.9893	18.5810	2.0527E-02
15	3302763471907603840	0.2579	+10.0905	57.2163	-15.0372	14.6607	0.9197	17.4677	2.7800E-02
16	3302347405538192768	0.1123	+9.0186	57.5283	-14.6794	13.5157	0.9866	18.1334	7.7986E-03
17	3302517627978790784	0.2305	+9.7887	58.3446	-13.4025	13.6600	0.8746	17.0933	1.1627E-02
18	3273949498390088448	0.2311	+6.2544	58.3769	-15.6878	15.0130	0.9952	17.1423	7.7895E-03
19	3259376124600082688	0.0439	+2.7632	63.5494	-18.0006	16.5966	1.0363	16.9342	1.0527E-02
20	3283413643508855168	0.4116	+3.2175	63.9090	-17.6916	16.5187	0.8983	18.2204	4.3555E-02
21	3283707732806011776	0.2904	+3.8795	66.0409	-16.9729	16.1823	1.0192	16.8527	7.6543E-03
22	3278904202725707776	0.4538	+0.6731	66.8839	-18.0428	16.9354	0.8860	18.3811	2.6335E-02
23	3205031181848570240	0.3451	-2.6066	69.8346	-19.8285	19.0347	0.6952	17.5299	6.7108E-03
24	3229172192289896576	0.5220	-1.8187	69.8390	-20.3993	19.0081	0.9991	19.1580	6.6485E-03
25	3225714404316322048	0.5186	-3.3168	72.0153	-20.3162	19.3406	0.9340	17.5908	1.3595E-02
26	3225088713480594304	0.1847	-3.0706	72.5461	-20.7489	19.8459	0.9562	15.6898	1.7710E-02
27	3188312385993123968	0.2624	-6.0464	72.9310	-23.3288	22.2830	0.7262	17.4658	7.0712E-03
28	3225017378367519232	0.1945	-3.3841	72.9781	-21.1877	20.1364	0.7722	18.1341	2.3440E-02
29	3212479479773005696	0.2639	-5.2492	73.6805	-22.6205	21.5271	0.6668	17.0226	2.9807E-02
30	3187421678493781888	0.3710	-6.0663	74.5026	-21.6876	20.4548	0.7595	17.7014	1.1591E-01
31	3183889733612983296	0.2107	-8.0801	75.1650	-24.2181	22.8004	0.9031	18.1802	5.9379E-03
32	3182335646943552000	0.3665	-9.8777	75.9863	-23.4187	22.8338	0.8467	17.0998	1.0542E-02
33	3183733710337675136	0.2786	-8.2173	76.5810	-22.5581	21.3874	0.8088	18.0632	6.5451E-02
34	318277115233055152	0.0302	-9.2063	76.6356	-21.4523	20.5276	1.1081	18.9625	6.5732E-03
35	2989805452906457216	0.2265	-11.1401	77.4576	-24.2242	23.2763	0.9121	18.4459	5.6177E-03
36	2985707611726244480	0.2369	-13.1102	80.3573	-23.6520	23.4954	0.7765	17.4529	6.0301E-03
37	2985448500643184896	0.3116	-13.5979	81.3864	-22.5934	22.6676	0.8775	17.9810	1.6029E-02
38	2985851682109593728	0.3032	-12.5971	81.5529	-23.6375	23.2202	0.8874	16.3023	3.2902E-02
39	2984359674895283072	0.4909	-14.7883	83.5002	-22.2270	22.7071	0.8658	18.4725	6.4990E-03
40	2971024729152562176	0.1691	-16.9745	85.2735	-23.8125	23.9815	0.8599	17.9274	6.5887E-03
41	2971248857726512128	0.1681	-15.7976	85.7306	-23.1975	22.6792	1.0410	18.7166	9.8945E-03
42	2967677373378985472	0.4029	-18.1238	86.3326	-23.3190	24.2962	0.7562	17.2588	2.2519E-02
43	2967743511577557120	0.4519	-17.9255	87.4169	-22.9684	24.0202	0.8708	17.7389	3.1562E-02
44	2967375007681446784	0.2755	-18.6319	87.6077	-23.5623	24.2818	0.7710	17.5950	3.9916E-02
45	2991860440139396608	-0.0381	-16.8690	88.2245	-22.8467	22.9447	0.9589	18.7355	6.0765E-03
46	2966606032438342144	0.2674	-19.4013	88.5997	-22.2754	23.4095	0.8417	18.0282	1.4813E-01
47	2966413828356833152	0.2144	-19.5051	88.8025	-22.2084	23.3199	0.7694	17.3525	2.0891E-01
48	2918181822364292736	0.2471	-20.3285	89.1767	-22.3439	24.2402	0.8385	18.1034	1.6488E-02
49	2990877854701797888	0.3134	-17.4093	90.4209	-23.6439	23.5650	0.9256	17.1479	1.0600E-02
50	2916935594654099712	0.3217	-22.3985	90.8435	-22.0852	24.1436	0.7733	17.7879	5.6818E-03
51	2917978004694480128	0.2612	-20.5596	90.9743	-22.0869	23.9064	0.7235	17.1207	8.3623E-02
52	2941157702670871680	0.4038	-20.9649	91.8675	-21.8820	23.8108	0.7327	16.6851	5.0665E-02
53	2941141931553193856	0.3032	-21.1686	92.2365	-21.8213	23.1047	0.8605	17.9485	1.6438E-01
54	2941295279065097472	0.2902	-20.4353	92.5552	-22.8800	24.2738	0.6464	16.0479	2.0424E-02
55	2937577417936027008	0.2063	-22.4331	93.8184	-20.6428	22.4657	0.7654	17.5514	1.1616E-01
56	2936748248729371008	0.3291	-22.9566	95.0570	-21.4088	23.8275	0.7250	16.8219	2.2029E-02
57	2937679290262547584	0.0609	-21.8367	95.3396	-20.4362	22.4033	0.9023	18.3712	8.8452E-03
58	2924361047651213184	0.3045	-24.2864	96.6325	-20.8322	23.3102	0.6946	17.0423	1.1522E-01
59	2923332351444848896	0.2326	-25.4506	98.1197	-18.9226	21.7545	0.8182	16.1500	5.3253E-02
60	2919762198531603456	0.2841	-27.6668	98.8488	-18.8438	22.7615	0.9272	18.1750	5.9658E-03
61	2923457523971828480	0.3593	-25.2914	99.9176	-20.4000	23.7148	0.8881	18.0914	1.4250E-02
62	2919619949213987200	0.2580	-27.6074	100.5084	-19.2244	22.0807	0.9075	18.6624	2.2055E-02
63	2918864520305483264	0.4388	-27.7485	101.3058	-18.7304	22.2778	0.9241	18.1616	1.3436E-01

Table C1. - continued

N	source_id	π (mas)	δ (deg)	α (deg)	μ_δ (mas yr ⁻¹)	$\mu_{\alpha*}$ (mas yr ⁻¹)	$G_{BP}-G_{RP}$ (mag)	G (mag)	χ_{sel} (yr ³ deg ⁻² pc ⁻¹ mas ⁻³)
64	2918802226100396032	0.3037	-27.9478	101.8551	-18.4146	21.9682	1.1722	18.6582	8.6932E-02
65	2919192204830525312	0.1634	-27.5619	102.0146	-18.6500	22.3833	0.7739	16.7921	8.5157E-02
66	5608974194743618304	0.1431	-29.0134	103.0615	-18.4799	22.6030	0.9807	17.2841	6.2600E-03
67	5604401257167040896	0.1817	-31.3957	106.9045	-16.2835	21.7660	0.9967	18.2635	5.6973E-03
68	5604387551929978624	0.1216	-31.4825	107.4312	-15.7999	21.3128	0.8960	17.8501	2.8356E-02
69	5604416031855199360	0.2044	-31.2087	107.7262	-16.2320	21.3956	1.0559	17.4261	3.0635E-02
70	5605860210317910656	0.1027	-31.2627	108.2240	-16.1830	21.3612	0.8866	18.1165	5.1754E-03
71	5605025887150553344	0.2347	-31.7202	109.0093	-15.7407	21.4371	0.8631	17.5631	1.4133E-02
72	5587654118824699136	-0.0611	-35.6350	115.3624	-13.8094	19.3400	1.7499	20.5729	1.1787E-03
73	5587324089239122688	-0.2146	-36.4645	117.2742	-12.9198	19.9370	1.5662	19.2243	9.6739E-04
74	5539044602383550720	0.4356	-37.2963	119.2984	-11.0610	19.3346	2.4144	19.6161	5.4508E-04
75	5424452710261263872	-0.2191	-43.1483	140.7367	-4.6507	12.3840	1.6736	19.5148	1.1320E-03
76	5424980029168882560	0.3051	-43.1169	142.9833	-4.7781	11.2861	1.6641	19.0377	6.2820E-03
77	5412717553938252544	0.1385	-44.1282	144.6515	-4.4577	11.2894	1.1298	18.8000	1.2108E-02
78	5412394400600530432	-0.0005	-45.1641	146.4960	-3.4355	10.2152	1.0007	19.0347	6.6114E-03
79	5411987340783459840	0.0278	-44.7558	147.9285	-4.5372	9.6447	1.2994	19.8551	3.5455E-03
80	5412063585038036096	0.1458	-44.7961	148.5284	-2.7358	8.7963	1.0250	19.5906	4.3700E-03
81	5411902609663942272	0.2299	-44.7107	149.0004	-3.4370	10.5574	1.4347	20.2248	4.8709E-03
82	5408678635415016576	0.2071	-46.0086	149.5061	-2.6238	9.9105	0.9979	17.5241	1.2022E-01
83	5411828465645835648	0.1680	-44.9974	149.6303	-2.9013	9.7088	1.0017	19.0311	1.5012E-01
84	5414808107804098432	0.4901	-45.2014	150.4793	-3.6007	9.8601	1.1010	20.3807	6.1875E-03
85	5408722242225130880	-0.4469	-46.0245	150.6442	-3.1488	9.1825	1.1029	19.4458	2.9276E-03
86	5414950318459476864	0.0050	-44.4130	150.9149	-3.2737	8.4006	1.0093	19.3326	4.7786E-03
87	5414797898662111744	0.0673	-44.8816	151.1779	-3.7119	8.8205	1.1339	20.1646	5.2609E-03
88	5414539822663808768	0.3201	-45.6822	151.4893	-2.5543	9.8544	0.9911	18.8864	3.3081E-02
89	5414564183718662016	0.3195	-45.5630	151.5356	-2.8157	8.5250	1.0473	19.2840	4.9625E-02
90	5414524021482764672	0.5664	-46.0519	151.5567	-2.8607	9.5367	1.0047	20.1461	9.0886E-03
91	5414568478687775616	0.0000	-45.4720	151.7814	-1.9550	9.4562	1.0643	19.8742	1.9126E-02
92	5414568203809849600	0.0741	-45.4956	151.8199	-2.5132	9.2889	0.9280	18.2477	2.2365E-01
93	5414470175475053440	0.0939	-46.0117	152.0382	-2.0447	8.5806	0.9803	18.2909	1.5857E-01
94	5407680210138297472	0.3190	-47.0962	152.1243	-2.1293	8.9009	1.0210	19.3478	6.8538E-03
95	5414514808777843968	0.1885	-45.7093	152.1831	-3.2370	7.6466	1.1894	20.4158	3.7572E-03
96	5414489799181004160	0.5853	-46.0332	152.2404	-2.4198	9.1888	1.0093	19.8201	2.8798E-02
97	5413703854532103040	0.5427	-46.4378	152.2645	-1.4183	8.4917	1.2109	19.5160	1.0050E-02
98	5413703403553024896	0.4628	-46.5002	152.2753	-1.3476	8.8112	1.1792	19.9166	8.7105E-03
99	5414501064881763584	0.5115	-45.8547	152.2918	-2.1137	9.1032	0.9609	18.9478	7.2786E-02
100	5413735804786642688	0.5939	-46.2623	152.4463	-1.7846	8.6619	1.1320	18.7962	1.1387E-02
101	5413736771158381056	0.3367	-46.1567	152.4470	-2.6524	8.7161	1.0038	19.3687	5.5646E-02
102	5413707531024130304	0.1513	-46.4227	152.4619	-2.1157	8.7608	1.4619	14.2777	1.2925E-01
103	5413686464201633024	0.3246	-46.6598	152.4782	-1.3244	9.1873	1.0932	19.8740	8.2365E-03
104	5413731922137962496	0.0330	-46.3127	152.6005	-1.4314	8.4122	1.0919	19.1534	1.7983E-02
105	5413746769842342912	-0.2302	-45.9664	152.6060	-1.4081	8.1404	0.9907	19.7287	3.9730E-03
106	5413694268165352704	0.1283	-46.5443	152.6153	-1.9544	8.7215	1.2519	16.1443	1.2764E+00
107	5413734224240710272	-0.0087	-46.1877	152.6410	-2.3915	8.6046	1.0492	18.7688	1.4529E-01
108	5413742268720312192	0.1306	-46.0010	152.6414	-2.2343	8.8286	1.2550	15.9851	1.8786E+00
109	5413721824672679552	0.2962	-46.2819	152.6430	-2.0587	8.7421	1.0147	18.2996	5.4112E-01
110	5413744364664262144	0.0805	-45.9321	152.6470	-3.1119	9.2018	0.9047	18.5161	9.4405E-03
111	5413743295212382208	0.3754	-45.9628	152.7251	-2.6614	8.3346	1.0136	18.5626	4.1028E-02
112	5413837204676171136	0.1280	-45.9449	152.7622	-2.3460	8.2183	1.0011	17.5443	1.7796E-02
113	5413720622081853824	0.2782	-46.3067	152.7667	-1.9144	8.6098	0.9940	17.6895	3.9211E-01
114	5413742951614948096	-0.5966	-46.0033	152.7743	-1.8458	8.8833	1.0139	19.5849	3.3428E-03
115	5413827996266328064	-0.0091	-45.8243	152.9341	-2.2238	8.5120	0.9132	17.3248	6.2819E-02
116	5413634654017870336	0.2101	-46.9412	152.9942	-2.0045	8.5502	1.2115	16.4645	1.9360E-01
117	5413835894705134208	-0.2688	-45.7065	153.0241	-1.8431	8.3532	0.9813	20.1126	5.5075E-03
118	5414389537468984064	0.1168	-44.3112	153.8987	-3.5476	8.3693	1.0589	18.4613	3.8191E-03
119	5414057892972812160	-0.0016	-45.2555	155.4083	-2.1204	7.7283	0.8449	17.6746	4.6860E-03
120	5365783216481459840	0.1342	-46.8392	155.8449	-1.4280	8.0469	1.1206	19.4101	1.7484E-02
121	5365391073082942336	0.2777	-47.3759	155.8568	-1.4592	8.4773	0.8594	17.7940	1.0584E-02
122	5365780398982621696	0.2621	-46.9529	155.8643	-1.3769	7.8673	1.0697	19.2203	2.2998E-02
123	5365399383845390976	-0.0230	-47.2051	155.9170	-1.2253	7.5164	0.9504	18.4153	1.0633E-02
124	5365789504313726080	0.0047	-46.7820	155.9225	-1.7586	6.9475	1.0258	19.1421	3.0141E-03
125	5365876365730787328	0.3279	-46.2400	155.9265	-2.0997	8.1445	0.9316	18.5095	5.3858E-02
126	5365792016874464640	0.0931	-46.6439	155.9438	-1.7115	8.1138	0.9518	17.1936	1.0490E-01

Table C1. - *continued*

N	source_id	π (mas)	δ (deg)	α (deg)	μ_δ (mas yr ⁻¹)	$\mu_{\alpha*}$ (mas yr ⁻¹)	$G_{BP}-G_{RP}$ (mag)	G (mag)	χ_{sel} (yr ³ deg ⁻² pc ⁻¹ mas ⁻³)
127	5365873445153019008	0.0975	-46.2453	155.9449	-1.3040	7.6397	1.3341	19.7425	5.1718E-03
128	5365865959033473152	0.2407	-46.3788	156.0361	-2.1501	8.4814	0.9965	19.1296	9.3859E-03
129	5365785965260649216	0.1707	-46.7892	156.0661	-1.4949	7.4019	0.9192	18.7294	1.9158E-02
130	5365819019327251840	0.5079	-46.3904	156.0674	-1.4804	7.4436	1.0385	19.3859	5.7243E-03
131	5365784178553932544	-0.1314	-46.9102	156.0887	-1.6961	7.5548	1.1499	19.4999	7.6562E-03
132	5365817163903821184	0.0751	-46.5291	156.1047	-1.6714	8.3504	0.9041	18.6001	1.5036E-02
133	5365825414540727296	0.1149	-46.3280	156.1078	-2.0940	7.8422	1.1164	19.7862	9.0039E-03
134	5365827476119277184	-0.0518	-46.2354	156.2146	-1.9832	7.0940	1.0906	19.5436	3.1556E-03
135	5365810261890643840	0.2137	-46.7570	156.2188	-2.0729	6.9264	0.7268	18.8097	2.9639E-03
136	5365921445707194624	0.2320	-46.1857	156.2351	-1.5871	7.4213	1.0728	19.0933	1.1313E-02
137	5365193706449182592	0.3000	-47.4672	156.2907	-1.2538	7.5130	0.8539	18.2828	2.5675E-02
138	5365768338714318080	0.7031	-47.0099	156.3480	-1.1768	8.0557	1.1333	19.4720	3.4492E-03
139	5365819775241396224	0.0269	-46.4617	156.3699	-2.0587	8.1793	0.9681	18.6001	1.4942E-02
140	5365190682792082048	0.1500	-47.5861	156.3725	-1.4167	8.1328	0.8341	18.3808	2.2653E-02
141	5365809437262578176	0.2534	-46.4901	156.4128	-1.7321	7.5130	1.0855	19.4212	8.7985E-03
142	5365578294999961344	0.4987	-47.1869	156.4923	-1.9379	7.6787	0.8898	18.8358	5.5409E-03
143	5365579016555060096	0.2704	-47.1131	156.5143	-1.9269	7.0518	1.0797	19.3789	4.2389E-03
144	5365576065920333440	0.1539	-47.1961	156.6824	-1.6095	7.6348	1.5148	12.9366	1.0524E+01
145	5365898355962610688	0.3840	-46.5396	156.7343	-1.5688	7.0853	0.9684	18.9476	5.4961E-03
146	5365601629562571008	0.2543	-47.0240	156.8280	-0.9371	7.3243	1.1609	18.9579	5.2161E-03
147	5365736178000020864	0.3027	-46.1942	157.4884	-2.2346	7.7748	0.9663	17.0385	2.0367E-02
148	5364616737729276928	0.3602	-47.7895	159.6636	-0.6013	7.2650	1.0342	19.2178	4.9192E-03
149	5366070189016080384	0.4429	-47.5857	160.3078	-1.1778	6.6145	1.1561	18.3634	7.2854E-03
150	5366058407925709568	-0.0212	-47.7929	160.3254	-1.1813	6.5427	0.9288	17.8935	7.3902E-03
151	5363031246257881984	0.4249	-48.2777	161.0511	-0.5582	6.8420	0.9608	18.1045	9.4285E-03
152	5363251045501068160	0.3074	-47.6732	163.6266	-1.0451	6.0923	0.9211	17.9304	2.4429E-02
153	5374364767295481856	0.1341	-47.8018	168.1795	-0.4224	4.5801	0.7357	18.7395	1.1996E-02
154	5374570105393379072	0.1369	-47.2856	169.4423	-0.8148	4.3892	1.2607	14.4835	1.2424E-01
155	5373850234514547712	0.2316	-47.6973	171.1533	-0.3389	3.6895	1.0015	19.0083	1.0363E-02
156	5373847481435744512	0.1238	-47.1102	171.3746	-1.1421	3.6006	1.0540	18.0519	9.0333E-03
157	5373628957800529280	0.1411	-47.6738	172.1138	-0.7113	4.0836	0.8235	18.1147	2.4378E-02
158	5375101959778889216	-0.2126	-47.3622	173.2150	-0.5569	3.3159	0.8618	19.1182	9.8719E-03
159	5375091376982888192	0.2061	-47.4674	173.5502	-0.5459	3.5834	0.8895	18.6912	4.3155E-02
160	5372062218149409536	0.1720	-47.9061	174.1886	-0.4939	3.0765	1.0942	19.4563	7.8447E-03
161	5372147915636764544	0.5759	-47.4353	174.6326	-0.5447	3.6150	0.7032	19.3034	9.9653E-03
162	5371948693572713856	-0.0380	-47.4375	175.3823	-1.2254	2.8094	0.9519	19.9073	7.7881E-03
163	5372345617270244480	0.0380	-46.9986	175.7310	-1.5697	3.1700	1.2063	20.0780	8.1299E-03
164	5372254082932197248	0.2239	-47.7630	176.1961	-0.4725	3.3897	1.0882	19.2860	2.2251E-02
165	5372296551563595520	-0.2300	-47.1799	176.3097	-0.4701	3.3724	0.9962	19.5314	2.4790E-02
166	5372386608438137600	-0.2060	-46.9739	176.5707	-1.1318	3.1125	1.0581	19.7879	4.4448E-02
167	5372378877496792064	-0.0659	-47.1248	176.6575	-1.2263	3.3820	0.7079	19.4287	1.3672E-02
168	5371655196988321152	0.7329	-46.8830	177.0731	-0.5633	3.7295	0.7188	20.2820	1.4290E-02
169	5377605302940159232	0.5001	-46.8489	177.7541	-0.1653	3.7658	0.9804	20.0362	1.3828E-02
170	5377724707328398592	0.3648	-46.4346	178.2477	-1.0006	3.7925	0.8342	20.0085	8.0794E-03